Analytic Redundancy for On-Line Fault Diagnosis in a Nuclear Reactor

Asok Ray,* Robert Geiger,† Mukund Desai,‡ and John Deyst§
The Charles Stark Draper Laboratory, Inc., Cambridge, Massachusetts

A computer-aided diagnostic technique has been applied to on-line signal validation in an operating nuclear reactor. To avoid installation of additional redundant sensors for the sole purpose of fault isolation, a real-time model of nuclear instrumentation and the thermal-hydraulic process in the primary coolant loop was developed and experimentally validated. The model provides analytically redundant information sufficient for isolation of failed sensors as well as for detection of abnormal plant operation and component malfunctioning.

Nomenclature

B = bias for sensor calibration
b = error bound for measurement
C = specific heat
F = mass flow rate of primary coolant
H = measurement matrix
K = product of heat transfer coefficient and area
ℓ = number of measurements
M = thermal mass
m = measurement
p = parity vector
Q = power or rate of energy flow
S = scale factor for measurement
T = temperature
t = time
V = projection matrix
v = sensor output in volts
w = weighting coefficient ($0 < w < 1$)
x = true value of a measured variable
ϵ = measurement noise
η = parameter associated with heat transfer
ξ = shim blade position
τ = time constant
χ = fraction of neutron power

Subscripts and Superscripts

a = ambient
c = cold leg
e = entrance
g = shield
h = hot leg
n = neutron power
o = outlet
p = primary coolant
r = reflector
s = secondary coolant
t = primary coolant at core tank
x = primary coolant at heat exchanger
$( )^*$ = nominal value
$(\hat{\ })$ = estimate

Introduction

IN complex industrial processes such as nuclear power plants, operational safety, reliability, and system performance can be improved by computerized fault diagnostics[1-6] which exploit all useful redundant information that is available in the plant. Redundancy is broadly classified as 1) direct—when two or more sensors are available for measurement of a process variable; and 2) analytic—when additional evaluation is analytically obtained from a mathematical model formulated on the basis of physical relationships among other direct or analytic measurements. These relationships may follow fundamental laws of physics such as mass, momentum, and energy equations, or they may be derived from the normal operating characteristics of an equipment. Analytic measurements may thus be used to supplement sensor redundancy for process variables of interest. To reliably identify the failure of a sensor measuring a scalar process variable such as power, flow, or temperature, at least triple redundancy is required. For example, when only dual redundancy is available, failure detection can be done, but reliable identification of the failed sensor is not usually possible. In addition to its use in isolating the failure of sensors, an analytic measurement allows detection of plant component failures and/or common mode failures, i.e., simultaneous and identical failures of two similar devices possibly due to a common cause.

In commercial nuclear power plants, there are a number of nonsafety related process variables that do not have triply redundant sensors, and these variables are often crucial for plant reliability and availability. Examples are feedwater flow and main steam flow on the secondary side of pressurized water reactor (PWR) plants.[7] In practice, installation of additional sensor hardware to achieve sufficient redundancy is often not feasible owing to several constraints such as cost, space limitations, and radioactive environments; analytic measurements may be the only source of supplemental redundancy for detection and/or isolation of plant component and sensor failures. On the other hand, the major requirements of an analytic relationship or mathematical model include 1) sufficient accuracy for reliable fault diagnostics under prescribed plant operations, and 2) appropriate execution time and memory requirements for on-line applications in a digital computer. Usually an analytic relationship or model can be structured to accommodate the valid measurements of other process variables (with sufficient sensor redundancy) as inputs. In that case, the computational requirements and errors of the model can be reduced.

This paper presents a technique for development of real-time process models that supplement sensor redundancy for fault diagnostics in industrial processes. As a proof-of-concept, on-line detection and isolation of sensor and plant component failures have been demonstrated in an operating nuclear reactor under steady-state and dynamic operations.

Background of the Fault Diagnostic Technique

The fault detection and isolation methodology[5,6] adopted in this study provides a unified, systematic procedure for

Received May 6, 1982; revision received Aug. 6, 1982.

*Staff Member.
†Research Fellow.
‡Staff Member. Member AIAA.
§Division Leader. Member AIAA.

redundancy management where relative consistencies among all direct and analytic measurements are taken into account in the framework of the parity space concept; a brief mathematical description is given in the Appendix. For a given set of ℓ scalar measurements, consistencies of $\ell(\ell-1)/2$ pairs are concurrently checked to obtain a multilevel characterization of each measurement as opposed to the usual bilevel fail/no fail status. An estimate of the measured variable is obtained from the largest consistent subset, and the inconsistent measurements, if any, are isolated.

In contrast to other approaches,[1-4] this fault detection and isolation (FDI) technique does not require a detailed knowledge of sensor and plant noise statistics, nor does it assume a specific pattern of noise distribution such as Gaussian. Instead, the FDI decisions are made on the basis of error bounds specific to individual measurements. The information on tolerances due to calibration, nonlinearities, scale factor errors, etc., that are usually available from the manufacturer's specifications, are sufficient to determine the error bounds.

The FDI technique is adaptable for on-line applications with mini- and microcomputers. The memory requirement is small and no multiplicative arithmetic operations are involved[5] for fault detection and isolation in scalar measurements; only a few multiplications are needed if an estimate is obtained as a (weighted) average of several consistent measurements instead of midvalue selection. In contrast, other FDI methods[2-4] need to solve a number of differential equations for recursive filters that require relatively larger computations, and the FDI decisions are more vulnerable to modeling errors due to changes in the assumed plant characteristics.

System Description

The test facility consists of a nuclear reactor equipped with adequate instrumentation and a minicomputer for exercising on-line fault diagnostic techniques. Detailed descriptions of the reactor configuration and instrumentation are given in Ref. 8. For illustration of the fault diagnostic problem, as limited to the primary coolant system, a simplified diagram is given in Fig. 1.

Nuclear Reactor MITR-II

The nuclear reactor MITR-II (Ref. 8) is heavy-water reflected, light-water cooled and moderated, and uses 27 flat-plate-type, finned, aluminum-clad fuel elements, containing highly enriched U^{235}. The reactor has a rated capacity of 5 MW_t and functions as a research and educational facility at MIT. The reactor power level is regulated by vertical movements of one regulating rod and a shim blade assembly consisting of six boron-impregnated stainless steel plates.

Heat generated by fission of U^{235} is removed by the primary coolant which is force-circulated by a pair of electrically driven centrifugal pumps, operating in parallel. The coolant enters the core tank at the bottom; it is directed upward through the fuel plates, and then exits rather slowly through the core shroud. The hot primary coolant is cooled in a bank of heat exchangers and returned to the core tank; typical hot leg and cold leg temperatures at normal load are 50 and 42°C, respectively. The heat exchangers transfer thermal energy from the primary to the secondary coolant, which, in turn, dissipates heat to the atmosphere by means of forced-air-circulated cooling towers.

Instrumentation

Four measurements of fission power are available from three neutron-flux sensors located at three separate locations around the core and a gamma-ray sensor that measures the radioactivity of the primary coolant in the outlet pipe. Four measurements of the primary coolant flow are obtained from the pressure differences across orifices and restrictions. Primary coolant temperatures are measured as follows: one

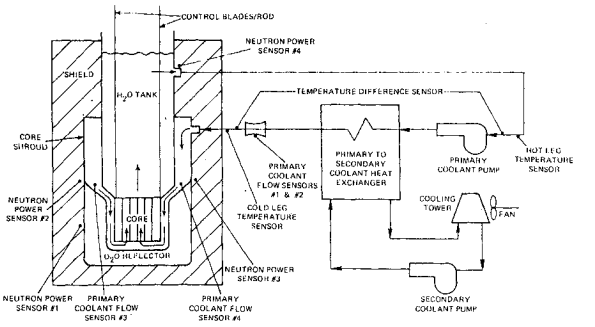

Fig. 1 Simplified schematic diagram for the nuclear reactor.

sensor for hot leg temperature, one sensor for cold leg temperature, and one sensor for temperature difference between the legs. In effect, two sources of temperature difference are available from direct measurements. All these measurements are available as voltage signals.

Data acquisition and on-line computation for fault diagnosis were performed by a MINC-11/23 minicomputer using FORTRAN and MACRO assembly language codes under the RT-11 operating system. Other instrumentation consists of analog to digital converters (ADC), filters, signal conditioners, and amplifiers for low level signals. The crucial sensors are buffered by signal isolators to eliminate the effects of any possible malfunctioning in the fault diagnostic equipment on the reactor operation.

Direct Redundancy—Sensor Models

Power Sensors

In this study, neutron power is defined as the total power produced by neutron induced fission and associated decay heat. There is no significant measurement delay associated with the three neutron flux sensors that are located around the core (see Fig. 1), whereas the gamma-ray sensor in the coolant outlet piping experiences considerable delay.

Calibration of neutron flux sensors is dependent on the neutron flux profile, which, in turn, is influenced by 1) fuel loading and depletion; 2) variations in fuel, moderator, and reflector temperatures; and 3) neutron absorber concentration.

Effects of fuel loading and depletion are slow and, therefore, do not need to be accounted for in real time, though periodic recalibration of the neutron flux sensors is required. In MITR-II, the variations in fuel, moderator, and reflector temperatures are not large enough to cause significant changes in neutron flux. Since MITR-II experiences weekly startup and shutdown, the variations in neutron absorption are due primarily to xenon poisoning. The flux changes due to xenon buildup have been shown to be negligible in an earlier study.[9] However, xenon poisoning also results in insertion of negative reactivity which is compensated for by partial withdrawal of shim blades, thus invoking a change in flux profile. To compensate for this change, scale factors for calibration of each neutron flux sensor were obtained as functions of shim blade position using the experimental data. Neutron power Q_n was derived from readings of the three neutron flux sensors via the linear relationship

$$Q_{ni} = S_i v_i + B_i \qquad i = 1,2,3 \tag{1}$$

The scale factor S_i of ith flux sensor is given by

$$S_i = S_i^* + S_{Ii}(\xi^* - \xi) \tag{2}$$

where ξ is the shim blade position; S_i^* is the scale factor at nominal blade position ξ^*; and S_{Ii} is the constant for scale factor compensation.

The operating principle of the gamma-ray sensor is measurement of the decay rate of N^{16} which is produced by neutron interaction with O^{16}. This sensor is calibrated for measurement of steady-state neutron power, taking into consideration a half life of 7.4 s for N^{16} and the transport delay due to coolant flow within the core tank. However, a change in neutron flux due to shim blade movement has no immediate effect on the sensor reading because of the transport delay associated with the time for the coolant to reach the sensor. To account for this effect, the error bound of the gamma-ray sensor is dynamically compensated as a linear function of the magnitude of the time derivative $\dot{T}_t$ of the primary coolant temperature in the core tank and the primary coolant flow $\hat{F}$.

Flow Sensors

The primary coolant flow is determined from measurements of pressure drops across orifices and restrictions. Since the density changes of subcooled water are not significant, for temperature changes in the operating range 20-55°C, the coolant flow can be assumed to be proportional to the square root of the measured pressure difference. Primary coolant flow is essentially constant under all operations, so the flow-pressure drop relations can be linearized about the normal operating point, thereby eliminating the repeated operations of square root.

Temperature Sensors

Temperature difference measurements between the hot and cold legs of the primary coolant are linear with respect to the sensor signals over the full operating range. The measurement lags in the sensors are insignificant in comparison to the process lags. The effects of transport delay due to fluid flow have been considered in the formulation of analytic redundancy presented in the next section. Sensors for measurements of secondary coolant and ambient temperatures used in the analytic redundancy are not available to the computer system.

Position Sensors

Sensors for measuring positions of the regulating rod and shim blades have linear characteristics over the full range.

Analytic Redundancy—Process Model

Figure 1 shows that sufficient direct redundancies exist for fault isolation and measurement validation for neutron power and primary coolant flow, but there is only dual redundancy for hot leg to cold leg temperature difference. Dual redundancy is sufficient for fault detection but inadequate for a fault isolation. This shortcoming can be circumvented if a third measurement of temperature difference can be analytically obtained using the physical relationships among other process variables, including the validated measurements of neutron power and primary coolant flow. Failure of one of the two temperature-difference sensors can thus be identified from the consistency between the good sensor and the analytic measurement. Similarly, an inconsistent analytic measurement along with mutually consistent sensors implies either identical failure of both sensors, known as common-mode failure, or malfunctioning of plant component(s), and/or incorrect information input to the model describing the analytical relationship. The actual cause of the inconsistency can usually be resolved using other additional information.

A dynamic model of the nuclear-thermal-hydraulic process has been developed to generate an analytical measurement for temperature-difference in real time, which is sufficiently accurate for fault detection and isolation. Figure 2 shows the structure of the model and causality among the process variables.

In addition to the lumped parameter approximation of partial differential equations, the major assumptions are 1) uniform fluid flow over pipe cross sections; 2) constant density of the primary coolant; 3) linear spatial distribution of temperature in the direction of fluid flow in the core and heat exchanger; 4) negligible thermal inertia of fuel plates relative to that of coolant in the core tank; and 5) fixed distribution of neutron power into the fuel plates, primary coolant, and reflector.

The development of model equations involves consideration of the fundamental law of energy conservation, semiempirical formulas for heat transfer, and radioactive decay relationships as described in the following sections.

Heat Transfer

Heat transfer Q_{pr} from primary coolant to reflector due to conduction and convection is approximated by the simple relation

$$Q_{pr} = K_{pr}(T_t - T_r) \tag{3}$$

where the parameter K_{pr} is the product of the lumped heat transfer coefficient and effective area. Similarly, heat transfers Q_{pg} from primary coolant to shield, Q_{rs} from reflector to secondary coolant, and Q_{ga} from shield to the environment that are also due to conduction and convection are approximated as

$$Q_{pg} = K_{pg}(T_t - T_g) \tag{4}$$

$$Q_{rs} = K_{rs}(T_r - T_s) \tag{5}$$

$$Q_{ga} = K_{ga}(T_g - T_a) \tag{6}$$

Heat transfer from primary to secondary coolant in the heat exchanger is a complex process determined by the configuration and nature of the tube surfaces. The effective heat transfer coefficient is dependent on fluid flow, particularly the primary coolant flow on the tube side. Assuming thermofluid parameters such as kinematic viscosity, thermal conductivity, and Prandtl number remain relatively unchanged in the range of operation; heat transfer from primary to secondary coolant is calculated from the log-mean temperature difference and an approximation of the Dittus-Boelter equation.[10]

$$Q_{ps} = K_{ps}[\eta + (1-\eta)(F^*/F)^{0.8}](T_x - T_s) \qquad 0<\eta<1 \tag{7}$$

Since the operation of MITR-II is presently restricted to constant primary coolant flow, Eq. (7) reduces to

$$Q_{ps} = K_{ps}(T_x - T_s) \tag{8}$$

Heat transfer rates Q_{ps} and Q_{pr} are large in comparison to Q_{pg}, Q_{rs}, and Q_{ga}; their effects on the model performance are discussed later.

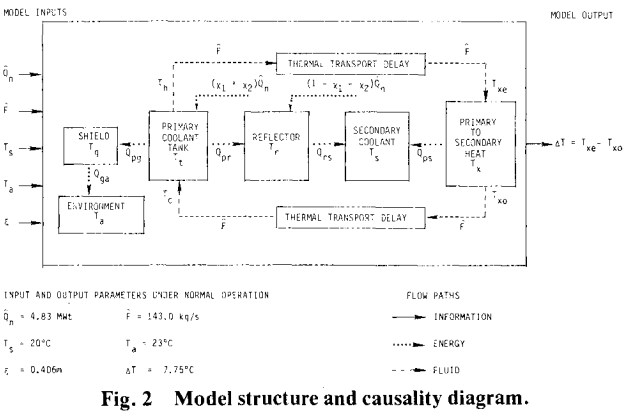

Fig. 2 Model structure and causality diagram.

Transport Delay

The temperature sensors are located close to the inlet and outlet of the heat exchanger. Therefore there are significant transport delays between 1) the core outlet and heat exchanger inlet, and 2) the heat exchanger outlet and core inlet temperatures.

Average primary coolant temperature in the core is approximated as the weighted average of the coolant inlet and outlet temperatures:

$$T_t = w_t T_c + (1 - w_t) T_n \qquad 0 < w_t < 1 \tag{9}$$

Hot leg temperature leaving the core is extrapolated from Eq. (9) as

$$T_h = (T_t - w_t T_c)/(1 - w_t) \qquad 0 < w_t < 1 \tag{10}$$

Similarly, coolant temperature at the heat exchanger outlet is extrapolated in terms of average temperature and delayed hot leg temperature as

$$T_{xo} = (T_x - w_x T_{xe})/(1 - w_x) \qquad 0 < w_x < 1 \tag{11}$$

Since coolant temperature transients are slow relative to the transport delays, finite-dimensional approximation of these delays is achieved by first-order lags instead of higher-order Pade expansion for computational efficiency. Thus delayed temperatures at heat exchanger and core inlets are governed by

$$\dot{T}_{xe} = (T_h - T_{xe})/\tau_h \tag{12}$$

$$\dot{T}_c = (T_{xo} - T_c)/\tau_c \tag{13}$$

Thermal Dynamics

The validated measurement $\hat{Q}_n$ of neutron power is assumed to be distributed as first, $\chi_1 \hat{Q}_n$, thermal power in the fuel plates, convected away by the primary coolant; second, $\chi_2 \hat{Q}_n$, radiative power into the primary coolant in the vicinity of the fuel plates; and third, $(1 - \chi_1 - \chi_2)\hat{Q}_n$, radiative power into the D_2O reflector. The difference between fuel plate and primary coolant temperatures is relatively small (less than 8°C), and the thermal capacitance of the coolant is large in comparison to that of the fuel plates in MITR-II. Therefore the dynamics of fuel plate and primary coolant temperatures have been modeled by a single thermal node in the core tank instead of two nodes (one for each temperature) coupled by convective heat transfer relations. The performance of the single-node model was verified with that of the two-node model; they were in close agreement. It is important to note that a single-node model may not be valid for commercial scale nuclear plants where the fuel temperature is significantly higher than the coolant temperature; in that case, additional equations are required for predicting fuel temperature and heat transfer from fuel to coolant.

Dynamics of average primary coolant temperature in the core are governed by

$$\dot{T}_t = [(\chi_1 + \chi_2)\hat{Q}_n - Q_{pr} - Q_{pg} - \hat{F}C_p(T_h - T_c)]/M_t \tag{14}$$

Similarly, the dynamics of reflector temperature are given by

$$\dot{T}_r = [(1 - \chi_1 - \chi_2)\hat{Q}_n + Q_{pr} - Q_{rs}]/M_r \tag{15}$$

Heat loss to the environment takes place through the layers of graphite and concrete in the shield that surrounds the core. It has a very large thermal capacitance. Owing to the weekly shutdown of MITR-II, the shield cools down during the weekend and gradually warms up to reach a thermal equilibrium during the week. Therefore the relatively slow dynamics of shield temperature are important for quasi-steady-state energy balance in the coolant although its effects on the thermal transients for neutron power changes due to control blade and regulating rod movements are insignificant. The governing equation for the thermal dynamics in the shield is

$$\dot{T}_g = (Q_{pg} - Q_{ga})/M_g \tag{16}$$

Dynamic energy balance in the primary to secondary coolant heat exchanger is given by

$$\dot{T}_x = [\hat{F}C_p(T_{xe} - T_{xo}) - Q_{ps}]/M_x \tag{17}$$

Table 1 Numerical values of model parameters

C_p	4.175×10^{-3} J/kg°C	w_t	0.5
		w_x	0.5
K_{ga}	2.96×10^3 W/°C		
K_{pg}	14.78×10^3 W/°C	τ_c	17 s
K_{ps}	179.00×10^3 W/°C	τ_h	21 s
K_{pr}	3.50×10^3 W/°C		
K_{rs}	1.40×10^3 W/°C	χ_1	0.9
		χ_2	0.088
M_g	0.36×10^9 J/°C		
M_r	3.6×10^6 J/°C		
M_t	3.5×10^6 J/°C		
M_x	3.0×10^6 J/°C		

Table 2 Model equations and system eigenvalues

$$\begin{bmatrix} \dot{T}_t \\ \dot{T}_x \\ \dot{T}_{xe} \\ \dot{T}_c \\ \dot{T}_r \\ \dot{T}_g \end{bmatrix} = \begin{bmatrix} -0.343 & 0 & 0 & 0.339 & 0.0010 & 0.0042 \\ 0 & -0.400 & 0.398 & 0 & 0 & 0 \\ 0.096 & 0 & -0.048 & -0.048 & 0 & 0 \\ 0 & 0.118 & -0.059 & -0.059 & 0 & 0 \\ 1.0 \times 10^{-3} & 0 & 0 & 0 & -1.4 \times 10^{-3} & 0 \\ 4.1 \times 10^{-5} & 0 & 0 & 0 & 0 & -4.9 \times 10^{-5} \end{bmatrix} \begin{bmatrix} T_t \\ T_x \\ T_{xe} \\ T_c \\ T_r \\ T_g \end{bmatrix} + \begin{bmatrix} 2.8 \times 10^{-4} & 0 & 0 \\ 0 & 0.060 & 0 \\ 0 & 0 & 0 \\ 0 & 0 & 0 \\ 3.3 \times 10^{-6} & 3.9 \times 10^{-4} & 0 \\ 0 & 0 & 0 \end{bmatrix} \begin{bmatrix} \hat{Q}_n \\ T_s \\ T_a \end{bmatrix}$$

$$\Delta T = [0 \quad -2 \quad 2 \quad 0 \quad 0 \quad 0] \quad [T_t \quad T_x \quad T_{xe} \quad T_c \quad T_r \quad T_g]^T$$

System eigenvalues, s^{-1}

Real	Imaginary
−0.4806	0.0
−0.1843	0.7030×10^{-1}
−0.1843	-0.7030×10^{-1}
-0.1540×10^{-2}	0.0
-0.5800×10^{-3}	0.0
-0.1364×10^{-4}	0.0

Parameter Evaluation

The model parameters were evaluated from engineering design specifications and experimental data. The parameters for heat transfer were obtained from the steady-state data. Constants for neutron power distribution into the three regions and weighting coefficients for temperature distribution in the core tank and heat exchanger were calculated from design specifications. Thermal capacitances and time constants were initially generated from design specifications and later updated by off-line parameter estimation using the transient data. Numerical values of the model parameters are listed in Table 1.

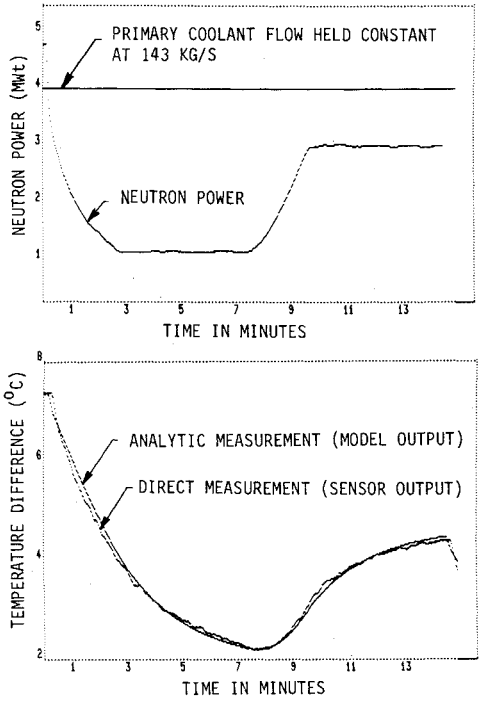

Fig. 3 a) Disturbance in neutron power. b) Comparison of direct and analytic measurements for hot leg to cold leg temperature difference.

Results and Discussion

A series of tests was conducted to validate the model in real time. For a constant coolant flow, the bilinearity in Eq. (14) can be eliminated. Therefore the linear model can be expressed in the form $\dot{x}=Ax+Bu$, $y=Cx+Du$, as shown in Table 2. The two smallest eigenvalues of the A matrix are strongly related to reflector and shield temperatures that have no major effects on the model performance except on the steady-state accuracy. The other four eigenvalues that include a complex pair are associated with the coupled thermal-hydraulic phenomena and transport delay in the primary coolant loop.

The analytic measurement of temperature difference closely agreed with the direct measurements under various transient and steady-state operations. As a typical example, Fig. 3 displays a comparison between the analytic measurement and the average of two direct measurements of temperature difference when large perturbations in neutron power were applied through movements of the shim blades with the primary coolant flow held constant. Initially, there is a slight mismatch due to approximation of transport delays by first-order lags. Later on, the agreement is very close, which signifies that the accuracy of the analytic measurement is comparable to that of a sensor.

The allowable error bounds for the measurements can be evaluated either by analyzing the test data or from the information on tolerances due to calibration, nonlinearity, scale factor, etc., available from the instrument manufacturers. At different power levels of MITR-II, steady-state data for all measurements were collected and analyzed for evaluating the noise statistics; the results showed that the measurement noise is practically independent of the reactor power level. The

Table 3 Expected values and covariance matrices

Neutron power sensors, MW

	No. 1	No. 2	No. 3	γ ray
Expected value:	4.806	4.842	4.814	4.847
Covariance matrix	0.1953×10^{-3}	0.7122×10^{-4}	0.6054×10^{-4}	0.2151×10^{-3}
		0.2080×10^{-2}	0.4308×10^{-3}	-0.1080×10^{-2}
			0.2207×10^{-3}	-0.2439×10^{-3}
				0.1171×10^{-1}

Primary coolant flow sensors, kg/s

	No. 1	No. 2	No. 3	No. 4
Expected value:	142.9	143.0	143.1	143.0
Covariance matrix	0.4958×10^{-1}	0.3219×10^{-3}	0.8232×10^{-3}	0.4381×10^{-2}
		0.3181×10^{-1}	0.6113×10^{-2}	-0.1305×10^{-1}
			0.2857	-0.4234×10^{-1}
				0.4541

Temperature difference measurements, °C

	Sensor 1	Sensor 2	Analytic
Expected value:	7.813	7.731	7.735
Covariance matrix	0.4430×10^{-1}	0.1068×10^{-1}	-0.1992×10^{-3}
		0.3116×10^{-1}	-0.2436×10^{-3}
			-0.1731×10^{-3}

expected values and covariance matrices of power, flow, and temperature difference (ΔT) measurements at full load are listed in Table 3, which shows that the measurements are correlated, indicating the possible presence of process noise. On the basis of the analyzed data, spatial location, and manufacturer's specifications, the error bounds (see Appendix) for all operating conditions were chosen in the ranges 0.05-0.25 MW, 0.5-2.0 kg/s, and 0.3-0.5°C for neutron power, primary coolant flow, and temperature difference measurements, respectively. In contrast to recently reported work,[6] individual measurements of a given process variable are allowed to have nonidentical error bounds. For example, the error bound for the gamma-ray sensor (see Fig. 1) is designed to be relaxed under transient conditions to prevent possible false alarms, whereas the remaining three power sensors are assigned invariant error bounds.

A series of tests were conducted to demonstrate the capability of the program for on-line fault diagnosis in the MITR-II using a MINC-11/23 minicomputer. The machine-executable form of the program requires a memory of approximately 20 kilobytes that include the libraries of FORTRAN and special real-time routines. The execution time is less than 130 ms/cycle if no messages are generated. Therefore sampling frequencies were chosen in the range 1-5 Hz, and the choices were made depending on the volume of the message display such that the sampling periods are not exceeded.

During the several-months-long tenure of the tests, there were practically no false alarms. During this period, a natural failure occurred in the hardware of one of the flow sensors. The failure was abrupt and of large magnitude. It was immediately isolated, and the flow estimate was obtained from the remaining three sensors.

To verify the fault diagnostics capability of the methodology, different types of sensor failures in excess of the error bounds were simulated while the reactor was in operation (with prior permission from the reactor safety committee). Typical cases are reported below.

Faulty Sensor Calibration

The scale factor for one of the ΔT sensors was increased on line such that the resulting offset exceeded its error bound by a modest amount. An inconsistency of this sensor with respect to the remaining sensor and the analytic measurement (that were mutually consistent) caused the isolation of the affected sensor as "high fail" within a few samples. Similar tests were successfully conducted with the power and flow sensors.

Gradual Drift

Drifts were introduced in the form of ramp functions in individual measurements. Appropriate alarms were received when the drifts exceeded the respective error bounds. On the average, delays in detection decreased with increased drift rates.

To demonstrate the effect of a common-mode sensor failure, an identical drift was induced in the bias of each ΔT sensor. Consequently, the analytic measurement of ΔT was isolated as it gradually became inconsistent with the pair of mutually consistent ΔT sensors. The implication is that one of the following two events occurred: 1) analytic ΔT is wrong due to changes in the assumed process characteristics or to an error in one or more inputs to the model (see Fig. 2); 2) the two ΔT sensors are identically faulty possibly due to a common cause. An inspection of all sensor readings, in this case, revealed a common-mode failure of the ΔT sensors.

Degraded Instrumentation

Random noises with zero means were added to several measurements. Alarm rates increased with larger noise to signal ratio.

Failed Sensors

Sensors were disconnected one at a time from the data acquisition system, resulting in immediate isolation of the affected sensor.

Abnormal Plant Operation

As a means of extracting radiation for experiments, the MITR-II contains a port through the D_2O reflector. When this port is opened, owing to changes in neutron flux distribution, the scale factor for one of the flux detectors is significantly altered, thus causing an alarm for faults. In this case, an estimate of neutron power is obtained as a weighted average of the remaining sensor outputs. The operator is thus alerted to the possibility that the port may have inadvertently been opened.

Conclusions

This paper presents the application of an on-line fault diagnostic methodology to the primary coolant system of an experimental nuclear reactor. The concepts of parity space and analytic redundancy are the essence of the algorithm. To augment redundancy, a dynamic model of the nuclear-thermal-hydraulic process has been developed to generate measurements of the coolant temperatures with accuracy comparable to that of the respective sensors. The model runs in real time as a part of the fault diagnostic algorithm and utilizes the validated measurements of neutron power and primary coolant flow as input parameters.

The methodology is suitable for fault diagnostics in commercial-scale nuclear and fossil power plants as well as in chemical and process industries.

Appendix: Fault Detection and Isolation Methodology

The underlying principle of the fault detection and isolation (FDI) methodology[5] is briefly described in this section. The redundant measurements for a scalar process variable such as reactor power can be modeled as

$$m = Hx + \epsilon \tag{A1}$$

where m is the $(\ell \times 1)$ array of measurements for the process variable whose true value is x. The array ϵ represents measurement noise such that, for normal functioning of each measurement, $|\epsilon_i| \le b_i$, the specified error bound with $i = 1,2,\ldots,\ell$. For scalar sensors, the measurement matrix can be chosen as $H = [1\ 1 \cdots 1]^T$ without loss of generality. Therefore any two measurements at the sampling instant n are defined to be consistent if

$$|m_i(n) - m_j(n)| \le b_i(n) + b_j(n) \qquad \begin{matrix} i = 1,2,\ldots,\ell \\ j = 1,2,\ldots\ell \end{matrix} \tag{A2}$$

The consistency of each pair of measurements can be determined solely on the basis of current observations or by sequential tests that rely on past observations as well. As occasional inconsistencies are likely to occur when no failures are present, sequential tests are useful in reducing the probability of false alarms.

Since the consistencies among the measurements should be independent of x, the true value of the process variable, the measurement vector m is projected onto the left null space of the measurement matrix, called the parity space, such that the variations in the underlying variable x are eliminated and only the effects of the noise vector ϵ are observed. The projection of m onto the parity space of dimension $(\ell - 1)$, known as the parity vector, is given as

$$p = Vm = V\epsilon \tag{A3}$$

where V is chosen such that its $(\ell - 1)$ rows form an or-

thonormal basis for the parity space, i.e.,

$$VH=0 \qquad VV^T=I_{\ell-l} \qquad V^TV=I_\ell-H(H^TH)^{-1}H^T \quad \text{(A4)}$$

For normal operations, when no measurements have failed, the parity vector p is small, reflecting acceptable errors in all measurements which are mutually consistent within the allowable error bounds. If a failure occurs, the parity vector grows in magnitude in the direction(s) associated with the failed measurement(s). An increase in the magnitude of the parity vector signifies detection of a failure, and its relative orientation with respect to the failure directions can be used to identify the failed measurement(s). Reference 1 provides a systematic approach to fault identification by concurrently checking the consistencies of all $\ell(\ell-1)/2$ pairs of measurements in terms of their error bounds. For example, consider three measurements, m_1, m_2, and m_3, for a process variable. If one of the measurements, say m_1, is faulty, then only one pair, namely, (m_2, m_3), will exhibit consistency, and consequently the measurement m_1 will be isolated. An estimate $\hat{x}$ of the measured variable can be evaluated asa weighted average of the consistent measurements m_2 and m_3. However, absence of any consistent pair signifies failure of at least two out of the three measurements where a fault can be detected but not isolated; in that case, it may not be possible to obtain an estimate $\hat{x}$. A geometric interpretation of this methodology, along with further details, is given in Ref. 5.

Acknowledgments

The authors acknowledge the benefits of discussion with Professor David Lanning and John Bernard. Cooperation of the personnel of the MIT Nuclear Reactor Laboratory during the experimentation phase is appreciated. This work was supported by the IR&D fund of The Charles Stark Draper Laboratory, Inc.

References

[1] Desai, M., Deckert, J.C., and Deyst, J., "Dual Sensor Failure Identification Using Analytic Redundancy," *AIAA Journal of Guidance and Control*, Vol. 2, No. 3, May-June, 1979, pp. 213-220.

[2] Tylee, J.L., "A Generalized Likelihood Approach to Detecting and Identifying Failures in Pressurizer Instrumentation," *Nuclear Technology*, Vol. 56, March 1982, pp. 484-492.

[3] Clark, R.N. and Campbell, B., "Instrument Fault Detection in a Pressurized Water Reactor Pressurizer," *Nuclear Technology*, Vol. 56, Jan. 1982, pp. 23-32.

[4] Kitamura, M., "Detection of Sensor Failures in Nuclear Plants Using Analytic Redundancy," *Transactions of the American Nuclear Society*, Vol. 34, June 1980, pp. 581-583.

[5] Desai, M. and Ray, A., "A Fault Detection and Isolation Methodology," *Proceedings of the 20th IEEE Conference on Decision and Control*, San Diego, Calif., Dec. 1981, pp. 1363-1369.

[6] Ray, A., Desai, M., and Deyst, J., "Fault Detection and Isolation in a Nuclear Reactor," *Journal of Energy*, Jan.-Feb. 1983, pp. 79-85.

[7] *On-Line Power Plant Signal Validation Technique*, Rept. No. EPRI NP-2110, Electric Power Research Institute, Palo Alto, Calif., Nov. 1981.

[8] *Reactor Systems Manual*, Rept. No. MITNRL-004, MIT, Cambridge, Mass., 1980.

[9] Bernard, J., "MITR-2 Fuel Management, Core Depletion and Analysis," Nuclear Engineering Thesis, MIT, Cambridge, Mass., June 1979.

[10] Holman, J.P., *Heat Transfer*, McGraw Hill, New York, 1976.